crystals

MDPI

Article

Liquid-Phase Epitaxial Growth and Characterization of Nd:$YAl_3(BO_3)_4$ Optical Waveguides

Yi Lu, Peter Dekker and Judith M. Dawes *

MQ Photonics, Department of Physics and Astronomy, Macquarie University, 2109 Sydney, Australia; coeus.lu@gmail.com (Y.L.); peter.dekker@mq.edu.au (P.D.)

* Correspondence: judith.dawes@mq.edu.au; Tel.: +61-298-508-903

Received: 16 December 2018; Accepted: 28 January 2019; Published: 1 February 2019

Abstract: We investigated the fabrication of neodymium doped thin film optical waveguide-based devices as potential active sources for planar integrated optics. Liquid-phase epitaxial growth was used to fabricate neodymium-doped yttrium aluminum borate films on compatible lattice-matched, un-doped yttrium aluminum borate substrates. We observed the refractive index contrast of the doped and un-doped crystal layers via differential interference contrast microscopy. In addition, characterization by X-ray powder diffraction, optical absorption and luminescence spectra demonstrated the crystal quality, uniformity and optical guiding of the resulting thin films.

Keywords: thin film crystal growth; epitaxial layer growth; multifunctional borate crystals; planar optical waveguides

1. Introduction

Integrated optics and photonics are increasingly important for optical signal processing in many applications. They rely on the development of compact, robust planar optical devices. Integrated optics employ waveguides as the building blocks for optical components, which are then connected into circuits [1]. In particular, integrated optical systems using waveguide-based components typically include active devices such as lasers and modulators that are integrated into photonic circuits. In each case, the structure must be designed to guide and confine the light within the active region of the device via the careful design of the refractive index contrast between the cladding and the active layer. Optical waveguides are described as single mode or multimode, based on the properties of the structure, as determined by the refractive index and dimensions of the guiding layer and substrate or cladding [2]. Active waveguide devices offer particular advantages over their bulk counterparts, because the optical confinement increases the intensity of the signal and pump light within the waveguide, hence ensuring that the amplification or nonlinear optical frequency conversion is more efficient than comparable bulk devices [3]. Here, we consider multimode active planar dielectric devices.

Fabrication of planar waveguide devices has been accomplished by a variety of approaches [3]. For example, the refractive index inside a dielectric material may be modified using nonlinear multiphoton processes [4,5], or ion-exchange [6]. In another approach, two crystals may be optically polished and then thermally bonded to achieve strong adhesion between the crystal layers [7]. This typically requires careful polishing to ensure that the active layer is sufficiently flat and thin. Epitaxial growth processes [8], such as liquid phase epitaxy (LPE) [9], pulsed laser deposition [10], molecular beam epitaxy (MBE) [11], hydrothermal epitaxy [12], metal oxide chemical vapor deposition (MOCVD) [13], and halide vapor phase epitaxy (HVPE) [14], enable the production of high-quality crystalline materials, which are practical for waveguide fabrication.

There has been long-standing interest in multifunctional-doped borate laser crystals [15–24], which are used in compact robust lasers emitting fundamental or self-frequency-doubled wavelengths,

with Q-switched, mode-locked or continuous wave operation. The thermal conductivity of these crystals facilitates the operation of the lasers at high power and in thin disk geometries [25–27]. In addition, un-doped borates have been adopted for nonlinear optics [28,29]. This has led to a new drive for improved growth techniques for these crystals. Various approaches to optimize the crystal growth—the choice, preparation, mixing of the flux, and the temperature profile—have been reported [15–17]. There is a balance between the relatively slow growth of the crystals, and the control of the crystal phase and uniformity, due to the formation of crystal twins [30,31]. However, following an early report of epitaxial film growth [32], there has been recent interest in developing borate crystals for waveguide devices that are compatible with integrated optics. This geometry enables the concentration of the light in the active layer to enhance both the amplification and the optical nonlinearity of the device [33–36].

The liquid phase epitaxial growth technique has several advantages compared with other waveguide fabrication techniques. The layers are grown isothermally with homogeneous composition, so the quality of the epitaxial layer is comparable with that of bulk materials. The interface between the thin film and the substrate exhibits a step profile in the refractive index, whereas other waveguide fabrication techniques typically lead to graded index profiles. Generally, the modes propagating inside a multimode step index profile structure have a uniform effective index, whereas for a graded index profile, different modes have a different effective index. The thickness of the waveguide structure can be controlled accurately by the growth duration and growth temperature. Finally, liquid phase epitaxy is adaptable for any single crystalline layer or active dopant, using an appropriate flux system and growth conditions [8].

We investigated liquid phase epitaxy as an effective growth method for Nd:$YAl_3(BO_3)_4$ (Nd:YAB) thin films on compatible lattice-matched un-doped borate substrates. The resulting films, whose lattice constants are consistent with R32 crystal symmetry, exhibit very good optical properties. Differential interference contrast microscopy, X-ray powder diffraction and optical absorption and luminescence spectra were used to characterize the optical quality and uniformity of these thin films.

2. Crystal Growth

2.1. Crystal Growth Methods

The flux system for the Nd:YAB epitaxial growth was chosen to be $K_2Mo_3O_{10}$ with excess Y_2O_3 and B_2O_3 [16]. This flux system offers advantages, because it has lower volatility than the PbF_2-$3B_2O_3$ flux system, and excess Y_2O_3 and B_2O_3 were added to the initial flux to suppress Al_5BO_9 inclusions and to compensate for the volatility of B_2O_3 during crystal growth [16]. The mix for the growth was calculated as 8 at. % Nd/(Nd + Y) with 24.4 wt. % of Nd:YAB in the solution. The solvent composition was 91.9 wt. % of $K_2Mo_3O_{10}$ + 5.4 wt. % B_2O_3 + 0.25 wt. % Y_2O_3. All the chemicals were obtained from local suppliers and heat-treated in a 300 °C furnace to remove adsorbed water before weighing. They were completely ground and mixed in the platinum crucible (5 cm diameter) and heated in an electric resistance furnace at 1150 °C for 24 h. The temperature was then dropped to about 1000 °C to find the actual saturation point by repeated seeding. The seed was settled to the mid part of the solution to ensure a homogeneous temperature gradient.

The substrate for the thin film growth needs to be selected carefully. It must permit reasonable lattice matching with the epitaxial layer to avoid strain due to lattice mismatch, and it must ensure a refractive index contrast, so that the active layer is the guiding layer with a higher refractive index. We selected un-doped $YAl_3(BO_3)_4$ (YAB), as it satisfies these criteria well. We also determined that a neodymium fraction of 8% permitted waveguide confinement, without excessive lattice mismatch. The calculated refractive index contrast for 8 at % Nd dopant is 0.0632 for n_o and 0.0608 for n_e [16]. Figure 1a shows the prismatic faces $\{11\bar{2}0\}$ and $\{2\bar{1}\bar{1}0\}$ and the rhombic face $\{01\bar{1}1\}$ for Nd:YAB, along with the crystal axes in Figure 1b. Previous liquid phase epitaxial growth of NdAB yielded thin films of good quality using $Gd_{0.59}La_{0.41}Al_3(BO_3)_4$ substrates with growth rates of around 1 μm/min [32].

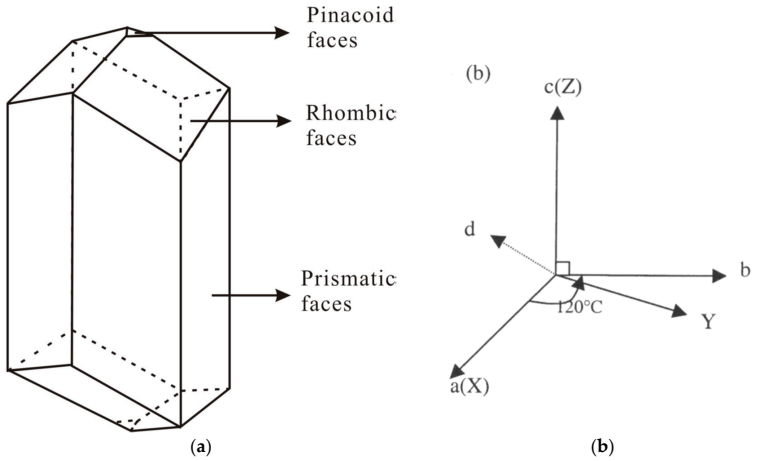

Figure 1. (**a**) The growth habit of Nd:YAB crystals and (**b**) the hexagonal crystal axes for the crystals.

The substrates were cut on the rhombic face $\{01\bar{1}1\}$ from bulk YAB crystals grown in our own laboratory and that of Professor N. Leonyuk. The surfaces of the substrates were left unpolished. The substrates were dipped vertically into the melt with platinum wire wrapped around the top of the substrates. The $\{01\bar{1}1\}$ cut pure YAB substrate (typical dimension 1 mm × 2 mm × 5 mm) was introduced and placed in the centre of the flux in the crucible.

Liquid phase epitaxial growth of thin films is typically similar to that of bulk crystals. The temperature is selected to be below the saturation point to allow the thermodynamic growth of layers with the same orientation as the substrate while immersed in a super-saturated solution. At conditions that are close to equilibrium, the deposition of the crystal on the substrate is slow and uniform. In our case, the temperature was initially set to 1 °C above the saturation point to smooth and dissolve the surface (which becomes the substrate–film interface) and the temperature was then ramped down to 4 °C below the saturation point (around 1000 °C) to start thin film growth. The growth rate was about 5 µm per hour at this temperature, as seen in Figure 2. This growth condition was chosen to ensure the thermodynamic growth regime and avoid any risk of spontaneous nucleation, which appears to occur for ΔT of 8 °C or more. After growth, the substrate was carefully removed from the flux and slowly cooled down to room temperature over 24 h. Bulk Nd:YAB crystals were also grown in our lab using the liquid phase epitaxy technique in the same solution. The solution mix was the same as for the thin film growth, with a small YAB seed.

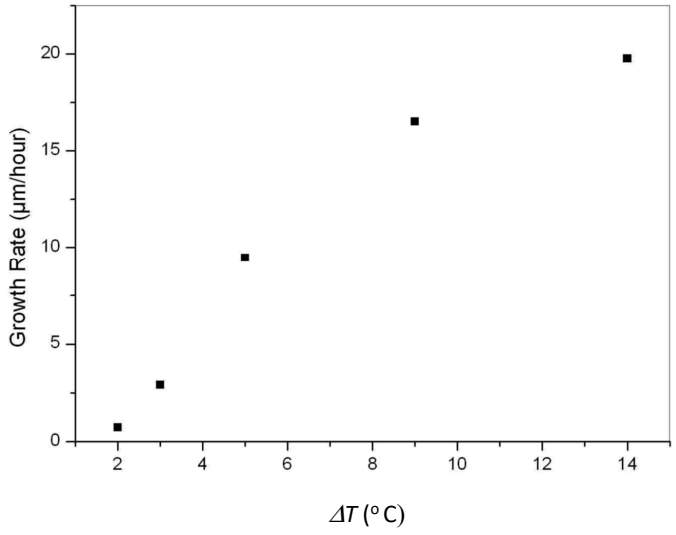

Figure 2. Nd:YAB crystal growth rate on the rhombic face seed crystal versus temperature below saturation ΔT (°C).

2.2. Results of Crystal Growth

Figure 3a shows an image of an as-grown Nd:YAB bulk crystal, with the growth facets visible, grown for two weeks under similar conditions as the thin films, with the temperature ramping down by 0.5 °C per day. Figure 3b shows an as-grown Nd:YAB crystalline thin film with un-doped YAB substrate that has been side-polished and imaged by a differential interference contrast microscope (Olympus BX60, Olympus Life Science, Sydney, Australia). The Nd:YAB thin film layer appears as a uniform, smooth blue stripe in the microscope image with a sharp change and an apparent phase contrast with the pure YAB substrate, which suggests a step-like refractive index profile. The film thickness was measured to be 71 ± 0.5 µm. The film shown in Figure 3b was obtained after epitaxial growth for 12 h at the conditions specified above. The as-grown thin film sample was transparent and homogeneous with a smooth surface. No noticeable crystallites of the monoclinic form of Nd:YAB were obtained, as discussed in Ref [35]. We attribute this to the moderate Nd dopant fraction and the lower temperature growth process that we used.

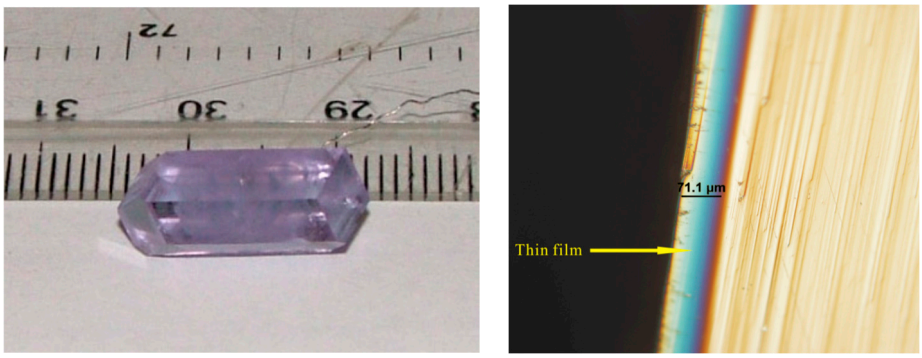

(**a**) (**b**)

Figure 3. (**a**) As-grown bulk Nd:YAB crystal and (**b**) differential interference contrast image of the Nd:YAB thin film and YAB substrate in cross-section.

3. Crystal Characterization Methods and Results

Crystal Characterization Results

X-ray powder diffraction was used to characterise the crystallographic structure, and the results were compared with the diffraction patterns in an existing database. The X-ray powder diffraction (XRD) pattern of ground Nd:YAB bulk crystals grown by top-seeded solution growth was measured using a D/max-rA type X-ray diffractometer (Rigaku, Rigaku Americas Corp, The Woodlands, TX USA) with CuKα radiation (λ = 1.54056 Å) at room temperature, and is shown in Figure 4. The X-ray powder diffraction pattern of the Nd:YAB crystals was found to be consistent with the reference pattern of $YAl_3(BO_3)_4$ and (JCPDS card No. 15-117) [37], indicating that the neodymium dopant does not significantly perturb the lattice and the crystal belongs to the R32 space group. The lattice parameters were calculated by the least-squares method.

According to the X-ray diffraction data, the calculated lattice constants of the Nd:YAB crystals were $a = b$ = 9.298 Å and c = 7.2406 Å. In comparison with the data presented in Ref [16], the measured lattice constants of the bulk Nd:YAB crystal were close to those of $Nd_{0.09}Y_{0.91}Al_3(BO_3)_4$, which were 9.295 Å and 7.236 Å. Thus our crystal properties are consistent with 9 at. % N dopant concentration within experimental error. Lattice constants of YAB crystals with different dopants are listed in Table 1. Assuming that the thin film has a similar Nd concentration to that of the bulk crystal, the lattice mismatch of the as-grown Nd:YAB thin film is about 0.11% and 0.2% for the lattice constants a and c, respectively. From optical microscopy and visual inspection, the Nd dopant distribution in the film appeared uniform. This is expected, as the solute concentration does not vary significantly during thin film growth.

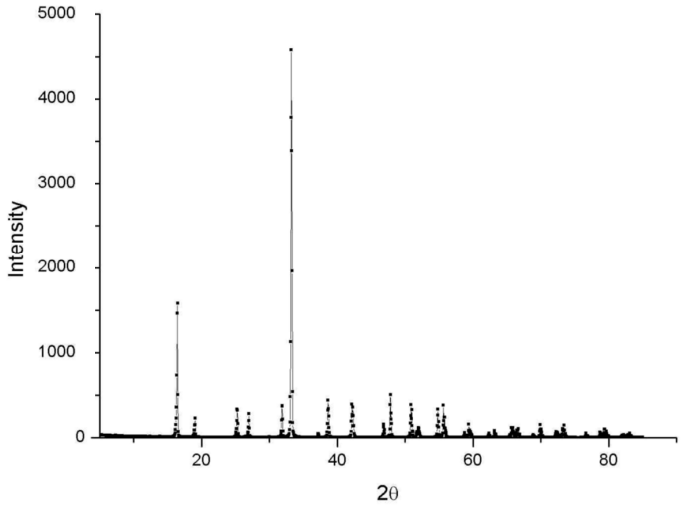

Figure 4. X-ray powder diffraction for as-grown Nd:YAB crystal.

Table 1. Lattice parameters of $YAl_3(BO_3)_4$.

Crystals	*a* (Å)	*c* (Å)	Reference
YAB (JCPDS No. 15-117)	9.2872	7.2433	[37]
$Nd_{0.09}Y_{0.91}Al_3(BO_3)_4$	9.295	7.236	[16]
$NdAl_3(BO_3)_4$	9.365	7.262	[16]
Nd:YAB crystal	9.298	7.2406	This work

The substrate crystal surface quality is shown in Figure 5a before thin film growth, and it shows the rough unpolished surface, which was smoothed in the initial period at a higher melt temperature. Figure 5b shows the as-grown crystalline film image in cross-section. The epitaxial growth results in a smooth surface with no additional crystallite formation. For the purposes of crystal characterization, the absorption spectrum of a 2 mm × 4 mm × 1.1 mm slice cut and polished from a bulk Nd:YAB crystal was measured using a Cary 5E spectrophotometer. This was compared with the absorption along the guiding direction of the epitaxial layer, as measured in the set up shown in Figure 6. Figure 7a shows the (unpolarised) absorption spectrum of bulk Nd:YAB (thickness 1.1 mm) in the wavelength range 300–1000 nm. There are six main absorption peaks in the spectrum at 360, 528, 588, 750, 809, and 882 nm, which may be assigned according to Reference [16]. The uncorrected absorption spectrum for the thin film is illustrated in Figure 7b. The absorption peak positions and features are similar to those for the bulk sample. The drifting base line is attributed to the wavelength response of the detector in the Ocean Optics HR2000 spectrometer.

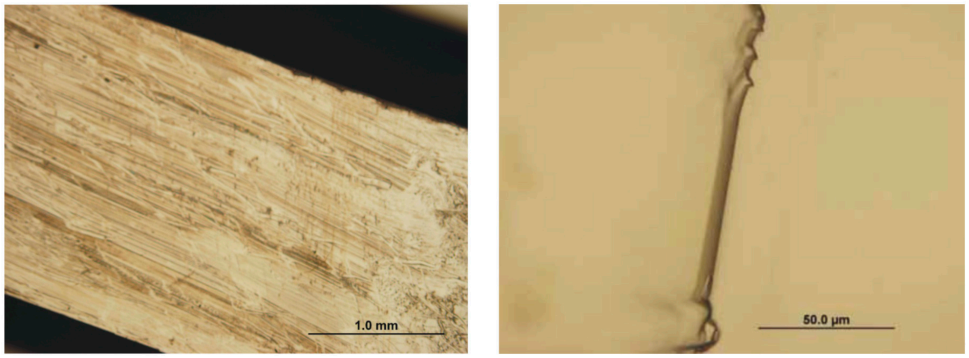

(**a**) (**b**)

Figure 5. (**a**) Microscope images of substrate surface (5×) and (**b**) after growth thin film surface (20×) for Nd:YAB on a YAB substrate. The substrate is held vertically in the flux.

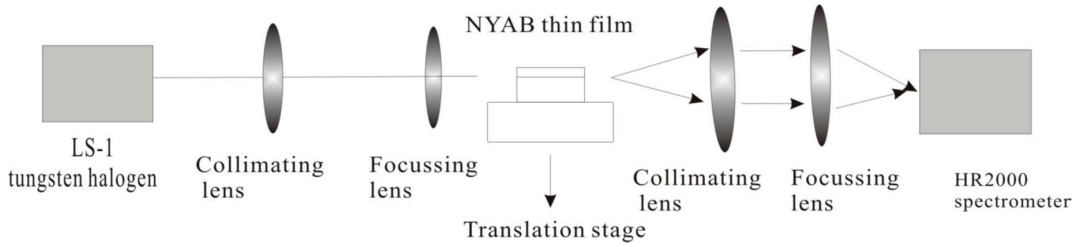

Figure 6. Experimental setup for measuring absorption spectra along guiding direction.

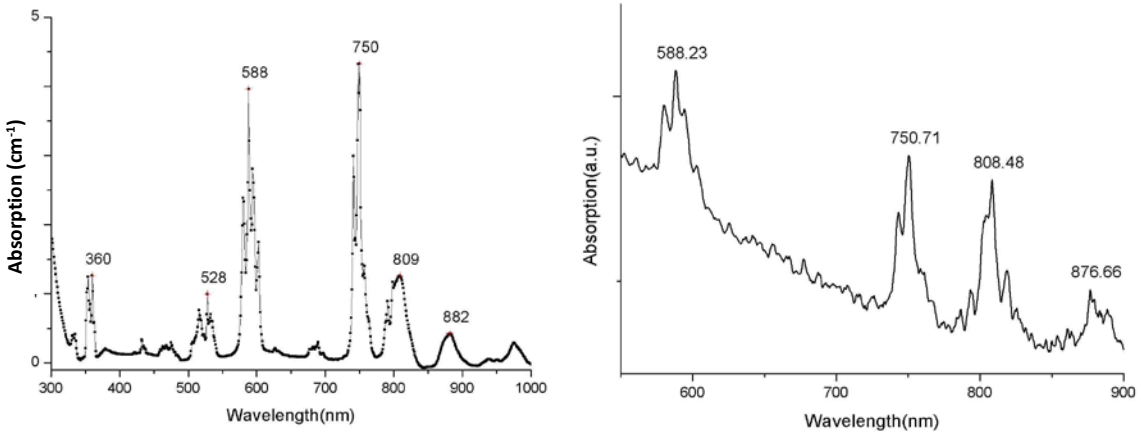

(**a**) (**b**)

Figure 7. (**a**) Absorption spectrum of a polished slice of bulk Nd:YAB and (**b**) uncorrected absorption spectrum of Nd:YAB crystalline thin film, along the guiding direction, showing intensity peaks at 588, 750 and 808 nm, attributed to transitions from $^4I_{9/2}$ to $^4G_{5/2}$, $^4F_{7/2}$ and $^2H_{9/2}$, respectively.

The near-infrared fluorescence spectra of the Nd:YAB thin film (thickness 71 µm), and a bulk Nd:YAB crystal sample at room temperature, are overlaid in Figure 8. This spectrum was obtained by coupling light from an 808 nm diode laser into the thin film and focussing the output by a lens into a fibre-coupled spectrometer. The 887 nm, 1062 nm and 1339 nm peaks correspond to the fluorescence of the $^4F_{3/2}$ level into the $^4I_{9/2}$, $^4I_{11/2}$, and $^4I_{13/2}$ multiplets, respectively. The room temperature fluorescence peak at 1062 nm is very strong, and the bandwidth (FWHM) of the 1062 nm peak is about 10 nm. The fluorescence spectrum of the thin film Nd:YAB crystal is well-correlated with that of the bulk Nd:YAB sample.

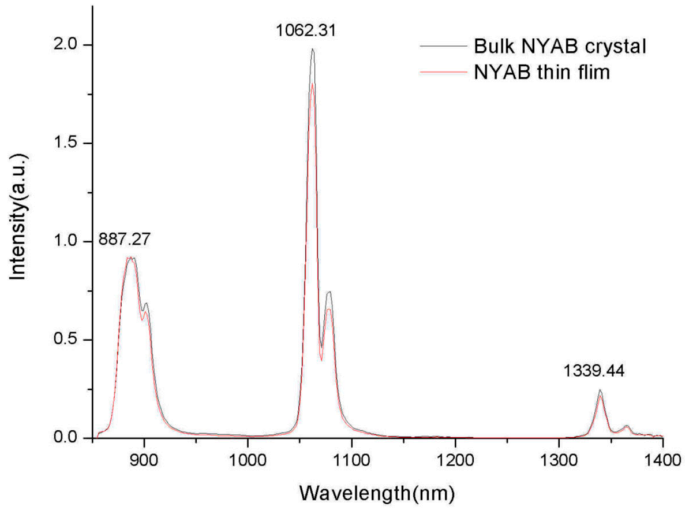

Figure 8. Luminescence spectrum of Nd:YAB thin film overlaid with that of the bulk Nd:YAB sample.

A near-field image of the Nd:YAB thin film luminescence emitted from the end of the waveguide, as longitudinally pumped by the 808 nm diode laser, is shown in Figure 9. This was captured by a CCD camera (Pulnix, JAI Pulnix, Sydney, Australia) through a 1064 nm band pass filter. The camera was coupled to a laser beam analyser (Spiricon LBA100A, Ophir-Spiricon Photonics, West North Logan, UT, USA). The luminescence image size is about 71 μm in the guided direction and 400 μm in the unguided direction. Two subsidiary images, probably due to back reflections, are also observable to the upper left. This image shows strong evidence of effective guiding within the epitaxial film layer.

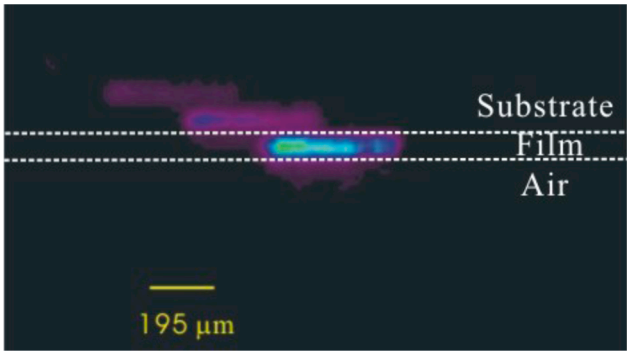

Figure 9. Luminescence image of Nd:YAB thin film (image artefacts to the upper left).

4. Discussion and Conclusions

Nd:YAB planar waveguides with 9% Nd dopant were successfully grown by the top-seeded solution method from the $K_2Mo_3O_{10}$ and B_2O_3 flux system. The growth rates were measured and the growth conditions and procedure were selected for high-quality film growth in the thermodynamic regime. Nd:YAB thin film layers were obtained at 4 °C below the saturation temperature, with a growth rate about 5 μm/h on an un-doped $\{01\bar{1}1\}$ YAB substrate. The growth of the thin films occurred over about 12 h, with additional time for cooling. The as-grown thin films have good surface and optical quality and homogeneity, and exhibit effective waveguiding of the strong luminescence at 1062 nm. Future measurements of optical gain and transmission losses in the devices are planned.

Author Contributions: Conceptualization J.M.D. and Y.L.; crystal growth methods and experiments Y.L.; crystal characterization Y.L. and P.D.; writing J.M.D. and Y.L. with editing by P.D.; and project administration J.M.D.

Funding: The authors acknowledge funding support to establish the crystal growth and characterization facility by Macquarie University and the Australian Research Council.

Acknowledgments: The authors acknowledge valuable advice and discussions on crystal growth and flux preparation from Nikolay Leonyuk and Robert Feigelson. Leonyuk provided bulk YAB crystals, which were used as substrates for the thin film growth.

Conflicts of Interest: The authors declare no conflict of interest.

References

1. Tien, P.K. Light waves in thin films and integrated optics. *Appl. Opt.* **1971**, *10*, 2395–2413. [CrossRef] [PubMed]
2. Snyder, A.W.; Love, J. *Optical Waveguide Theory*; Chapman and Hall: London, UK, 1983; pp. 6–26, ISBN 0-412-24250-8.
3. Mackenzie, J.I. Dielectric solid state planar waveguide lasers: A review. *IEEE J. Sel. Top. Quantum Electron.* **2007**, *13*, 626–637. [CrossRef]
4. Chen, F.; Vazquez de Aldana, J.R. Optical waveguides in crystalline dielectric materials produced by femtosecond-laser micromachining. *Laser Photonics Rev.* **2014**, *8*, 251–275. [CrossRef]
5. Ams, M.; Marshall, G.D.; Dekker, P.; Piper, J.A.; Withford, M.J. Ultrafast laser-written active devices. *Laser Photonics Rev.* **2009**, *3*, 535–544. [CrossRef]

6. Honkanen, S.; West, B.R.; Tliniemi, S.; Madasamy, P.; Morrell, M.; Auxier, J.; Geraghty, D. Recent advances in ion exchanged glass waveguides and devices. *Phys. Chem. Glass. Eur. J. Glass Sci. Technol. B* **2006**, *47*, 110–120.
7. Brown, C.T.A.; Bonner, C.L.; Warburton, T.J.; Shepherd, D.P.; Tropper, A.C.; Hanna, D.C.; Meissner, H.E. Thermally bonded planar waveguide lasers. *Appl. Phys. Lett.* **1997**, *71*, 1139–1141. [CrossRef]
8. Capper, P.; Irvine, S.; Joyce, T. Epitaxial Crystal Growth: Methods and Materials. In *Springer Handbook of Electronic and Photonic Materials*; Springer Handbooks; Kasap, S., Capper, P., Eds.; Springer: Cham, Switzerland, 2017.
9. Ferrand, B.; Chambaz, B.; Couchaud, M. Liquid phase epitaxy: A versatile technique for the development of miniature optical components in single crystal dielectric media. *Opt. Mater.* **1999**, *11*, 101–114. [CrossRef]
10. Beecher, S.J.; Grant-Jacob, J.A.; Hua, P.; Prentice, J.J.; Eason, R.W.; Shepherd, D.P.; Mackenzie, J.I. Ytterbium-doped-garnet crystal waveguide lasers grown by pulsed laser deposition. *Opt. Mater. Express* **2017**, *7*, 1628–1633. [CrossRef]
11. Cho, A.Y. Advances in Molecular Beam Epitaxy. *J. Cryst. Growth* **1991**, *111*, 1–13. [CrossRef]
12. Terry, R.J.; McMillen, C.D.; Chen, X.; Wen, Y.; Zhu, L.; Chumanov, G.; Kolis, J.W. Hydrothermal single crystal growth and second harmonic generation of Li_2SiO_3, Li_2GeO_3, and $Li_2Si_2O_5$. *J. Cryst. Growth* **2018**, *493*, 58–64. [CrossRef]
13. Sun, H.; Li, K.H.; Torres Castanedo, C.G.; Okur, S.; Tompa, G.S.; Salagaj, T.; Lopatin, S.; Genovese, A.; Li, X. HCl Flow-Induced Phase Change of α-, β-, and ε-Ga_2O_3 Films Grown by MOCVD. *Cryst. Growth Des.* **2018**, *18*, 2370–2376. [CrossRef]
14. Tassev, V.; Vangala, S.; Peterson, R.; Kimani, M.; Snure, M.; Markov, I. Homo and heteroepitaxial growth and study of orientation-patterned GaP for nonlinear frequency conversion devices. *Proc. SPIE* **2016**, *9731*, 97310G, "Nonlinear Frequency Generation and Conversion: Materials, Devices, and Applications XV, (4 March 2016); Vodopyanov, K.L.; Schepler, K.L.; Eds". [CrossRef]
15. Ballman, A.A. A new series of synthetic borates isostructural with the carbonate mineral huntite. *Am. Mineral.* **1962**, *47*, 1380–1383.
16. Leonyuk, N.I.; Leonyuk, L.I. Growth and characterization of $RM_3(BO_3)_4$ crystals. *Prog. Cryst. Growth Charact.* **1995**, *31*, 179–278. [CrossRef]
17. Wang, P.; Dawes, J.M.; Dekker, P.; Knowles, D.S.; Piper, J.A.; Lu, B.S. Growth and evaluation of ytterbium doped yttrium aluminum borate as a potential self-doubling laser crystal. *J. Opt. Soc. Am. B* **1999**, *16*, 63–69. [CrossRef]
18. Jaque, D.; Enguita, O.; Garcia Sole, J.; Jiang, A.D.; Luo, Z.D. Infrared continuous wave laser gain in neodymium aluminum borate: A promising candidate for microchip diode-pumped solid-state lasers. *Appl. Phys. Lett.* **2000**, *76*, 2176–2178. [CrossRef]
19. Wang, P.; Dekker, P.; Dawes, J.M.; Piper, J.A.; Liu, Y.G.; Wang, J.Y. Efficient continuous wave self-frequency doubling green diode pumped Yb:YAB lasers. *Opt. Lett.* **2000**, *25*, 731–733. [CrossRef] [PubMed]
20. Dekker, P.; Dawes, J.M.; Piper, J.A.; Liu, Y.G.; Wang, J.Y. 1.1W CW self-frequency doubled diode-pumped Yb:$YAl_3(BO_3)_4$ laser. *Opt. Commun.* **2001**, *195*, 431–436. [CrossRef]
21. Lederer, M.J.; Hildebrandt, M.; Kolev, V.Z.; LutherDavies, B.; Taylor, B.; Dawes, J.M.; Dekker, P.; Piper, J.A.; Tan, H.H.; Jagadish, C. Passive mode locking of a self-frequency doubling Yb:$YAl_3(BO_3)_4$ laser. *Opt. Lett.* **2002**, *27*, 436–438. [CrossRef]
22. Dekker, P.; Dawes, J.M.; Piper, J.A. 2.27 W Q-switched self-doubling Yb:YAB laser with controllable pulse length. *J. Opt. Soc. Am. B* **2005**, *22*, 378–384. [CrossRef]
23. Chen, Y.J.; Lin, Y.F.; Gong, X.H.; Tan, Q.G.; Luo, Z.D.; Huang, Y.D. 2.0 W diode-pumped Er,Yb:$YAl_3(BO_3)_4$ efficient 1.5 m laser crystal. *Appl. Phys. Lett.* **2006**, *89*, 241111. [CrossRef]
24. Lagatsky, A.A.; Sibbett, W.; Kisel, V.E.; Troshin, A.E.; Tolstik, N.A.; Kuleshov, N.V.; Leonyuk, N.L.; Zhukov, A.E.; Rafailov, E.U. Diode-pumped passively mode locked Er,Yb:$YAl_3(BO_3)_4$ laser at 1.5–1.6 m. *Opt. Lett.* **2008**, *33*, 83–85. [CrossRef] [PubMed]
25. Blows, J.L.; Dekker, P.; Wang, P.; Dawes, J.M.; Omatsu, T. Thermal lensing measurements and thermal conductivity of Yb:YAB. *Appl. Phys. B* **2003**, *76*, 289–292. [CrossRef]
26. Liu, J.; Mateos, X.; Zhang, H.J.; Li, J.; Wang, J.Y.; Petrov, V. High power laser performance of Yb:$YAl_3(BO_3)_4$ crystals cut along the crystallographic axes. *IEEE J. Quantum Electron.* **2007**, *43*, 385–390. [CrossRef]

27. Weichelt, B.; Rumpet, M.; Voss, A.; Wesemann, V.; Rytz, D.; Abdou Ahmed, M.; Graf, T. Yb:$YAl_3(BO_3)_4$ as gain material in thin disk oscillators: Demonstration of 109 W of IR output power. *Opt Expr.* **2013**, *21*, 25709. [CrossRef] [PubMed]
28. Yu, X.; Yue, Y.; Yao, J.; Hu, Z.G. $YAl_3(BO_3)_4$ crystal growth and characterization. *J. Cryst. Growth* **2010**, *312*, 3029–3033. [CrossRef]
29. Yu, J.; Liu, L.; Zhai, N.; Zhang, X.; Wang, G.; Wang, X.; Chen, C. Crystal growth and optical properties of $YAl_3(BO_3)_4$ for UV applications. *J. Cryst. Growth* **2012**, *341*, 61–65. [CrossRef]
30. Dekker, P.; Dawes, J.M. Characterisation of nonlinear conversion and crystal quality in Nd and Yb doped YAB. *Opt. Expr.* **2004**, *12*, 5922–5930. [CrossRef]
31. Dekker, P.; Dawes, J.M. Twinning and natural quasi-phase matching in Yb:YAB. *Appl. Phys. B* **2006**, *83*, 267. [CrossRef]
32. Lutz, F.; Leiss, M.; Muller, J. Epitaxy of $NdAl_3(BO_3)_4$ for thin film miniature lasers. *J. Cryst. Growth* **1979**, *47*, 130–132. [CrossRef]
33. Volkova, E.; Leonyuk, N. Growth of Yb:$YAl_3(BO_3)_4$ thin films by liquid-phase epitaxy. *J. Cryst. Growth* **2005**, *275*, e2467–e2470. [CrossRef]
34. Volkova, E.; Markin, V.; Leonyuk, N.I. High temperature growth and characterization of (Er,Yb):$YAl_3(BO_3)_4$ single crystal layers. *J. Cryst. Growth* **2017**, *468*, 258–261. [CrossRef]
35. Volkova, E.; Maltsev, V.; Kolganova, O.; Leonyuk, N.I. High temperature growth and characterization of Er,Yb:$YAl_3(BO_3)_4$ and $NdAl_3(BO_3)_4$ epitaxial layers. *J. Cryst. Growth* **2014**, *401*, 547–549. [CrossRef]
36. Tolstik, N.; Heinrich, S.; Kahn, A.; Volkova, E.; Maltsev, V.; Kuleshov, V.; Huber, G.; Leonyuk, N.I. High temperature growth and spectroscopic characterization of Er,Yb:$YAl_3(BO_3)_4$ epitaxial thin layers. *Opt. Mater.* **2010**, *32*, 1377–1379. [CrossRef]
37. Mills, A.D. Crystallographic data for new rare earth borate compounds $RX_3(BO_3)_4$. *Inorg. Chem.* **1962**, *1*, 960–961. [CrossRef]